ISSN 1027-4510, Journal of Surface Investigation: X-ray, Synchrotron and Neutron Techniques, 2017, Vol. 11, No. 6, pp. 1329–1337. © Pleiades Publishing, Ltd., 2017.

The Properties and Residual Stress of Argon arc Cladding Metal by Low Temperature Martensitic Transformation Powder[1]

Xizhang Chen[a, b, *], Ke Hu[a, c], and Sanbao Lin[b]

[a] *School of Mechanical and Electrical Engineering, Wenzhou University, Wenzhou, Zhejiang, 325025 China*

[b] *State Key Lab of Advanced Welding and Joining, Harbin Institute of Technology, Haerbin, Heilongjiang, 150001 China*

[c] *Zhejiang Provincial Key Laboratory of Laser Processing Robot/Key Laboratory of Laser Precision Processing & Detection, Wenzhou, Zhejiang, 325035 China*

**e-mail: chenxizhang@wzu.edu.cn*

Received March 14, 2017

Abstract—Martensitic Fe-based metal was achieved by argon arc surface cladding using self-developed low-temperature phase transformation (LTT) powders. Residual stress (RS), retained austenite (RA) content, hardness and wear resistance of the cladding layer under different powder compositions were tested. Meanwhile, the phase composition, microstructure and wear mechanism of the cladding metal were also analyzed. The results show that under suitable process parameters, the cladding layer and the substrate are metallurgical bonding without crack and porosity. The microstructure of the cladding layer is mainly lath martensite with less RA distributed on. Due to the volume expansion during phase transformation from austenite to martensite at about 200°C degree, large compressive RS is produced within the cladding metals, which has effectively compensated the tensile RS result from thermal shrinkage. The compressive RS reaches maximum of −361 MPa, and the average RA in the cladding layer is 10.85% for powder with composition of 10% Cr and 8% Ni. The hardness of the cladding layer is 2.6 times higher than that of the matrix material, which could reach up to 557.2 HV. The wear resistance of the surface cladding layer is nearly 57 times higher than that of the base material, which has the most excellent comprehensive performance.

Keywords: surface cladding, phase transformation, volume expansion, residual stress, wear resistance

DOI: 10.1134/S1027451017060222

1. INTRODUCTION

In industrial production, one of the important reasons that leads to the damage or failure of parts is surface wear, which causes hundreds of billions of economic losses to a country every year. Adopting advanced surface hardening technology to repair damaged parts on surface or synthesizing the required wear resistant coating on the surface of ordinary materials can significantly extend the service life of the product and reduce cost [1, 2]. In recent years, more and more researchers focus on in-situ synthesis of high hardness and wear resistant coatings from the view point of welding technology and hard phase particles [3–6]. Although the hardness and wear resistance of the cladding layer formed by hard phase particles are greatly improved, the tendency of crack is larger and the coating need to be preheated before cladding. The heating temperature of cladding layer is high and the cooling rate is fast, which can cause the thermal strain of the cladding layer and heat-affected zone (HAZ). Shrinkage of cladding metal always results in tensile residual stress (RS) in both the cladding layer and HAZ, which promotes the brittle fracture, stress corrosion cracking tendency and reduce the fatigue resistance of the cladding layer [7–11]. Therefore, it is necessary to eliminate the tensile RS to improve the life of the parts. At present, many post treatments are used to balance the tensile RS, such as post-weld heat treatment, shock, vibration method [12–14]. However, most of these methods increase the workload and cost, and it is hard to apply post treatment to some special parts in the actual production. Phase transformation under the constraint conditions occurred during cooling, in turn, the ferrite (A_1 ~ 550°C), pearlite (A_1 ~ 550°C), bainite (550°C ~ M_s), martensite (M_s ~ M_f) are formed, which leads to the volume expansion and compressive stress. The RS within the cladding metal is mainly determined by the tensile stress caused by the thermal contraction and the compressive stress generated by the phase transformation expansion. Due to the different volumes of each phase, the volume expansion during the phase transformation is not uniform. For carbon steel with 0.1%C, the microstructure at room temperature after phase transformation probably is ferrite, pearlite, bainite and martensite, and their volume expands by 4.58, 4.62, 4.71, and 4.80%

[1] The article is published in the original.

Table 1. Chemical compositions of S235 steel (wt %)

Base metal	C	Mn	Si	S	P	Fe
S235	0.14–0.22	0.30–0.65	≤0.30	≤0.05	≤0.045	Bal.

compared with the austenite, respectively [15]. So during the phase transformation, the volume of austenite is the smallest and the martensitic volume is the largest. It is an economical and efficient way to balance the tensile stress through volume expansion during phase transformation from austenite to martensitic. However, the phase transition temperature of steel is usually higher than 450°C, and the material is in elastic or elastic-plastic state. When the phase transition is finished, the volume expansion of the phase transformation will be fully recovered or partially recovered, the phase transformation stress is transient in the temperature range [16, 17]. It is required to improve the stability of austenite and reduce the temperature of the phase transition in the cladding layer, so that the martensitic transformation occurs at lower temperatures [18]. Low temperature martensitic transformation (LTT) alloy materials have been widely concerned and developed rapidly after being put forward in 1998 [19]. The LTT and conventional welding wire were used in the butt welding of high strength steel by Ohta Akihiko, the results showed that the fatigue strength of the welded joint by the LTT welding wire is increased by 100% [20]. Martinez Diez et al using Mn element instead of Ni element in the LTT alloy materials due to the relatively high cost of Ni, the results show that the Mn element also has the function of reducing the phase transition temperature and compressive RS is also obtained in the welded joint [21]. Research on steel pressure vessel welding by Camilleri Duncan et al. showed that the LTT welding wire effectively reduce the RS and deformation of the welded joint [22]. The angular distortion of T welded joint is studied by Mikami Y. et al. and the results showed that the angular deformation of the LTT welding joint is significantly less than that of the traditional welding wire [23]. The martensite start temperature (M_s) is mainly influenced by C, Mn, Cr, Ni, Mo [24, 25]. The equation (1) as shown can be used to evaluate the influence of alloy elements on the M_s [26]:

$$M_s(^\circ\mathrm{C}) = 561 - 474\mathrm{C} - 33\mathrm{Mn} - 17\mathrm{Cr} - 17\mathrm{Ni} - 21\mathrm{Mo}. \quad (1)$$

Research on LTT materials mainly concentrated welding technology with wire filler, less on cladding by powder, in fact, powder is also common used in cladding, additive manufacturing, the microstructure, properties and residual stress are also important for the cladding metals. The research in this paper focus on the RA and RS of cladding metal by power melting, and the effects of RA/RS on wear resistance, which is also less focused in welding technology. The LTT alloy powders with different ratios were in situ synthesis deposited on the S235 steel by argon arc cladding to obtain martensite. The compressive RS within the cladding metal is obtained due to the volume expansion of martensitic transformation, the hardness and wear resistance of the cladding layer are improved. The microstructure of cladding layer is observed, the effect of the RS, RA on hardness and wear resistance is investigated. The wear mechanism of the cladding layer is also analyzed to understand how the wear resistance is improved.

2. EXPERIMENTAL

2.1. Materials

The matrix material is S235 steel with the size of 100 × 100 × 10 mm^3. The chemical components of S235 steel are shown in Table 1. The alloy powders of cladding layer are mainly Fe–Cr–Ni alloy with the particle size of 23 μm according to the equation (1). In order to investigate the effect of the RS on the hardness and wear resistance of the cladding layer, three kinds of LTT alloy powders with different Cr/Ni ratios were designed, as shown in Table 2.

2.2. Cladding Process

The matrix material S235 is polished, then cleaned with anhydrous alcohol and acetone to remove the surface grease and rust. We put the weighed alloy powders according to the ratio of Table 1 into a planetary ball mill for four hours to make the composition uni-

Table 2. Chemical compositions of the laser cladding coatings (wt %) and the evaluated M_s (°C)

No	C	Si	Mn	Cr	Ni	Mo	V	Cu	Ti	Nb	B	Fe	M_s
1#	0.1	0.2	0.5	12	10	0.3	0.2	0.5	0.2	0.01	0.002	Bal	116.8
2#	0.1	0.2	0.5	10	8	0.3	0.2	0.5	0.2	0.01	0.002	Bal	184.8
3#	0.1	0.2	0.5	8	6	0.3	0.2	0.5	0.2	0.01	0.002	Bal	252.8

form, and the speed of ball milling is 150 round/min. In order to prevent the oxidation of metal powder in the process of ball milling, proper amount of anhydrous alcohol that just enough to immerse the metal powder is poured into the ball. After the end of the ball milling, the metal powder with anhydrous alcohol was put into the oven with a temperature of 80°C, and the door of the oven was kept open to prevent the explosion. The milled powder with a thickness of 1.2 mm is pre-layed on the base material by sodium silicate solution. We placed the sample into a vacuum drying oven with temperature set to 150°C for 2 hours and then dried in the air to room temperature. The coating is deposited on base metal with an argon tungsten arc, and single pass multilayer cladding was used to reduce the effect of the dilution rate. Before argon arc cladding, the first layer should be polished and cleaned. Argon arc cladding process parameters were: the current was 170 A, the speed of cladding rate was 60 mm/min and the argon flow rate is 12 L/min. The schematic diagram of the argon arc cladding process with the preset powder method is shown on Fig. 1.

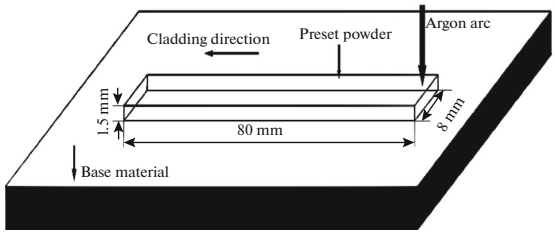

Fig. 1. Schematic diagram of argon arc cladding process with preset powder method.

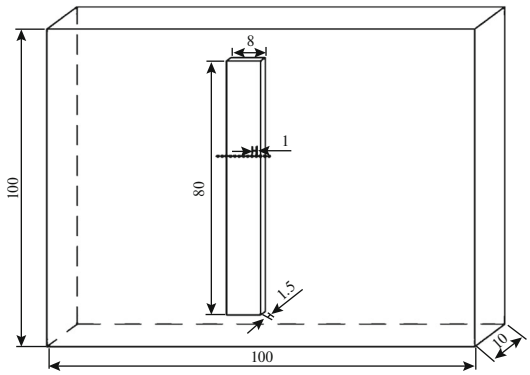

Fig. 2. Testing locations of the RS and RA.

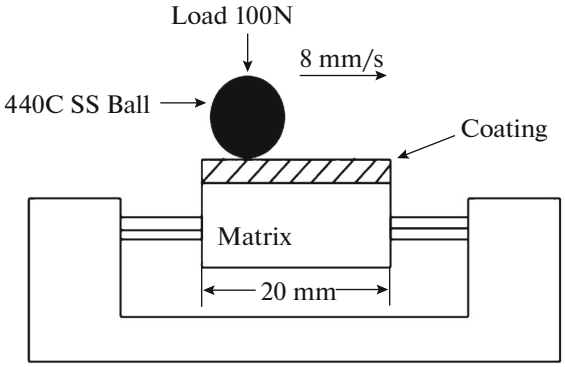

Fig. 3. Testing setup of sliding friction and wear.

2.3. Analysis Method

Starting from the center line of the cladding layer after electrolytic polishing, the RS and RA are tested by the X-350A type X-ray stress tester every 1mm along the direction perpendicular to the cladding metal. A method of fixed ψ with the angle from 0° to 45° and the 2θ scan angle from 151°–162° is used to measure. The high voltage of x-ray tube was 20KV and the current was 5mA. The diffraction crystal plane was (211) by Cr target. Figure 2 shows the schematic diagram of the RS and RA test locations. After being polished by metallographic sandpaper, the cross section of the cladding layer with the size of $10 \times 10 \times 8$ mm^3 was etched by a solution of 10 g $FeCl_3$ + 30 mL HCl + 120 mL H_2O for about 15 s. The micro-structure of the cladding metal was characterized by Axio Vert-A1 optical microscope (OM) and JEOL-JSM-7001F scanning electron microscope (SEM). The phase structure was analyzed by X-ray diffraction (XRD) using a D/max-2500/PC diffraction instrument. The micro-hardness from deposited layer to base material was measured by a HVS-1000 micro hardness tester with a load of 9.8N for 15s. The wear resistance at room temperature of the cladding metal was measured using MFT-5000 type friction and wear testing machine. The size of wear pattern is $20 \times 10 \times 10$ mm^3. The friction pair was 440C stainless steel ball with a diameter of 9.524 mm. The sliding speed of the friction pair was 8 mm/s with a load of 100 N. The time of wear was 60 minutes. The principle diagram of friction and wear experiment is shown in Fig. 3. The wear weight loss of the specimens at different time periods were measured using an electronic balance with an accuracy of 0.1 mg. The morphology of the cladding metal was observed by SEM, and the wear mechanism was analyzed.

3. RESULTS AND DISCUSSION

3.1. Microstructure

Figure 4 shows the microstructures of the argon arc cladding metal achieved with three different LTT alloy powders. As shown in Figs. 4a, 4c, 4e, the microstructure of the deposited metal is mainly composed of martensite and intercellular retained austenite (RA). The amounts of RA are measured in the following X-ray stress tester experiments (Fig. 7). The SEM was used to study the morphology of martensite in the cladding

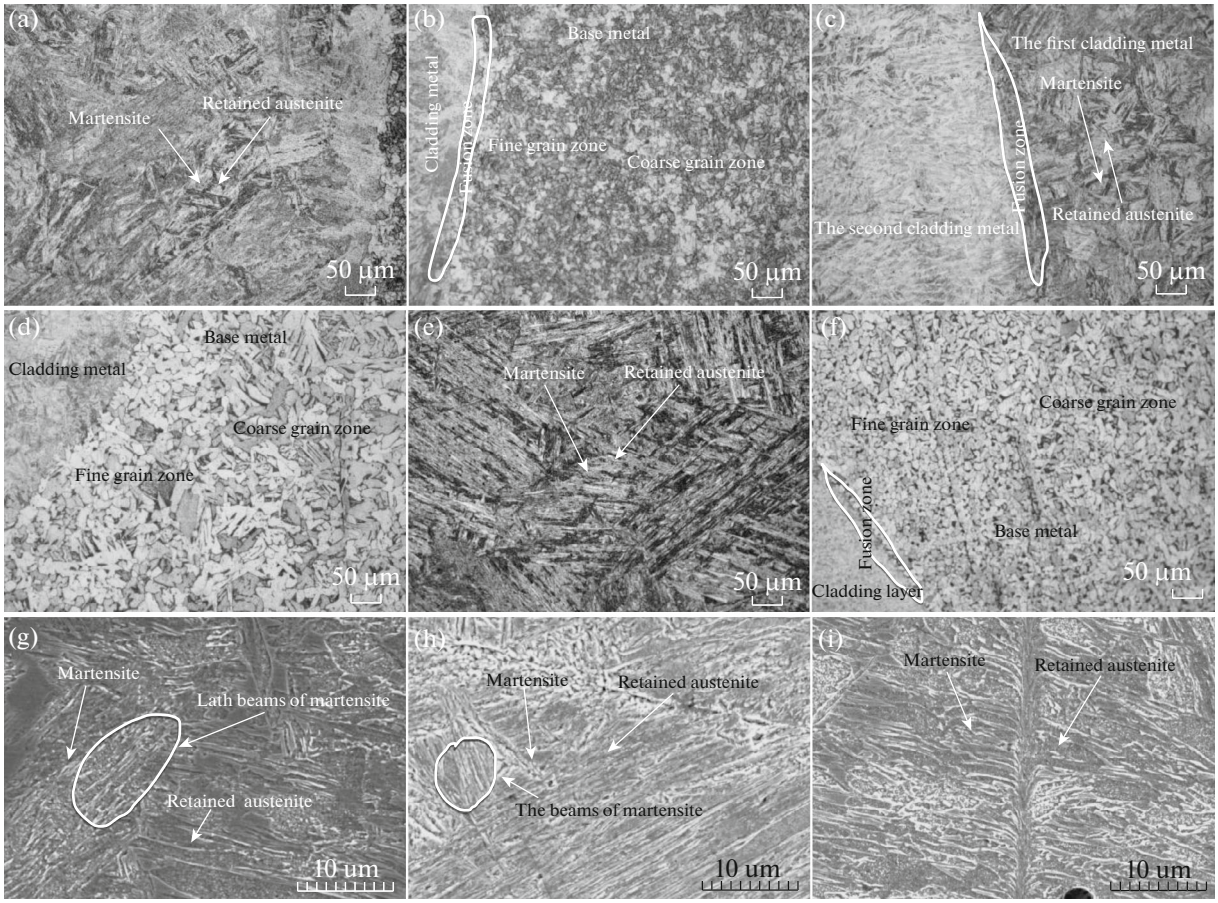

Fig. 4. Microstructure of argon arc cladding sample obtained by OM (a–f) and SEM (g–i). (a) OM of the cladding layer with 12%Cr, 10%Ni, (b) OM of the heat affected zone with 12%Cr, 10%Ni, (c) OM of cladding layer with 10%Cr, 8%Ni, (d) OM of the heat affected zone with 10%Cr, 8%Ni, (e) OM of the cladding layer with 8%Cr, 6%Ni, (f) OM of the heat affected zone with 8%Cr, 6%Ni, (g) SEM graph of the cladding layer with 12%Cr, 10%Ni, (h) SEM graph of the cladding layer with 10%Cr, 8%Ni, (i) SEM graph of the cladding layer with 8%Cr, 6%Ni.

metal more clearly. SEM graph of Figs. 4g–4i shows that the adjacent lath martensite with little phase difference is roughly parallel to each other, which forms a lath beam. When the two martensite slabs with different phase intersect with each other, a slight floating convex phenomenon can be seen in the intersection surface. The RA with polygonal grains is distributed between the lath martensite. As shown in Figs. 4b, 4d, 4f, the metallurgical bonding without crack and porosity between the cladding metal and the base metal has been formed. Due to the influence of the heat source, a heat affected zone (HAZ) which is an inhomogeneous continuum with a gradient of microstructure and properties is formed in the base metal [27]. The distribution schematic diagram of HAZ is shown in Fig. 5. The base metal near the fusion zone is not melted during arc cladding, but it will also be subject to a high temperature, resulting in the neighboring metal to be in a state of overheating and grains of the base metal near the fusion line grow up. Evenly coarse structure is formed after cooling to room temperature. Adjacent to the overheated zone is a normalized zone, the heat source induces phase transition recrystallization and the uniform and fine microstructure is obtained after cooling to room temperature. When the second layer cladding metal is deposited on the first

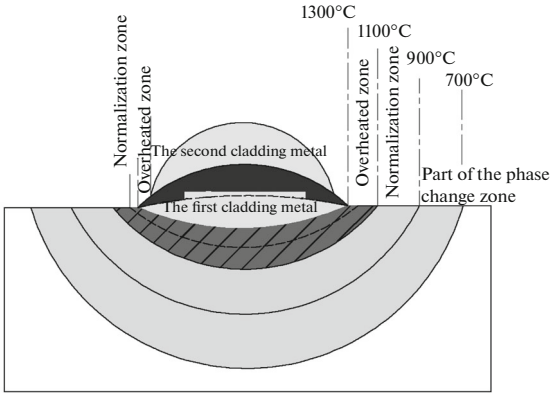

Fig. 5. Distribution schematic diagram of HAZ.

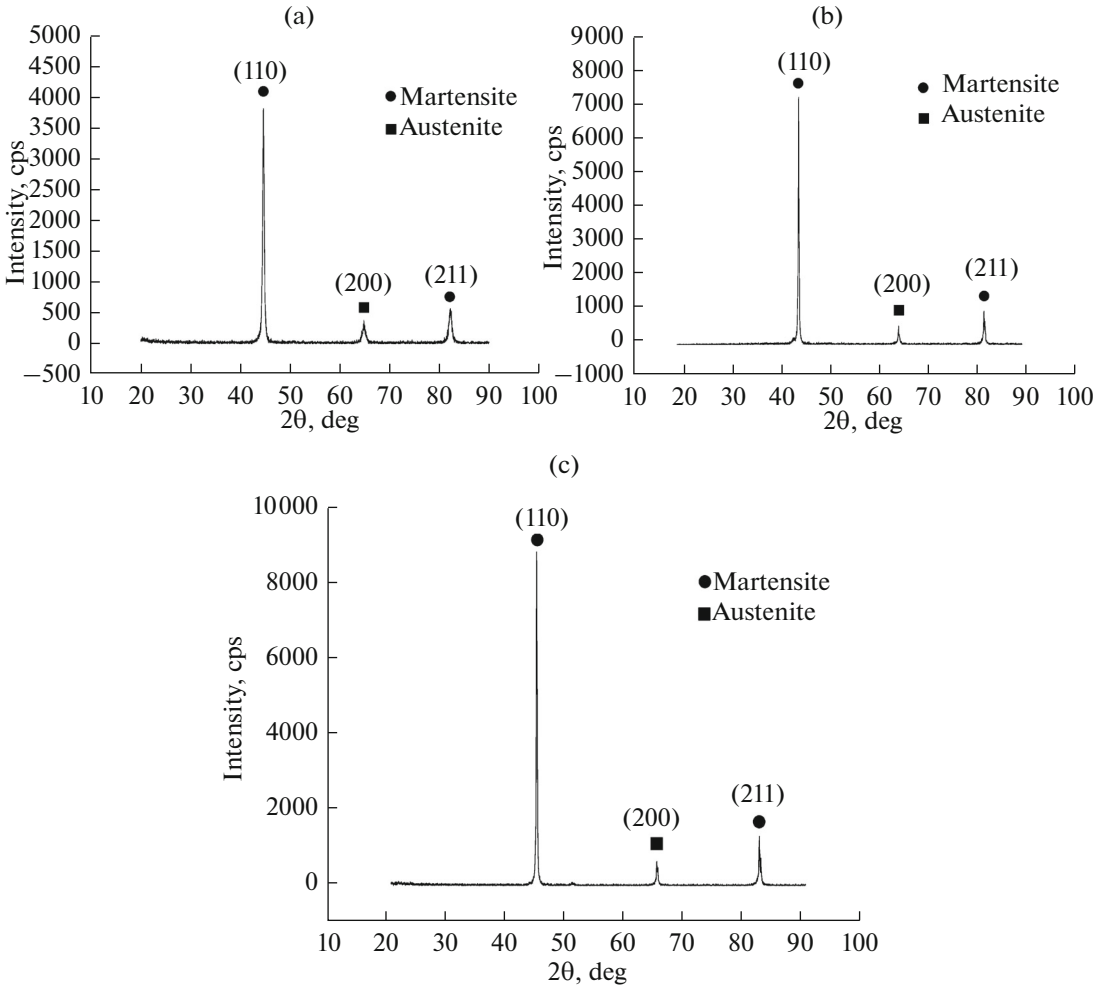

Fig. 6. XRD diffraction patterns of three groups of deposited layers: (a) 12%Cr, 10%Ni, (b) 10%Cr, 8%Ni, (c) 8% Cr, 6%Ni.

layer cladding metal, the arc heat source makes a part of the overheated zone of the HAZ in a phase transition recrystallization region. Finally, compared with the overheated zone by the first cladding metal, the coarse grain of this part is refined.

3.2. XRD Analysis

Figure 6 shows the X-ray diffraction pattern of the cladding layer with three different LTT alloy powders on the surface of S235 steel. Combined with the metallographic microstructure, as shown in the X-ray diffraction pattern, three groups of LTT alloy powders of the deposited layer are mainly composed of martensite and a small amount of residual austenite.

As shown in Fig. 6c, the Full Width Half Maximum (FWHM) of (110) diffraction peak is the widest, about 0.207°. The FWHM of (110) diffraction peak is the narrowest, about 0.204 from Fig. 6a. Because of the martensite is a kind of solid solution of carbon in the α-Fe, the interstitial carbon atoms can cause asymmetric lattice distortion, resulting in non-uniform stress field. The stress field can interact with the dislocations in the grain, which hinders the movement of the dislocation and increases the density of the dislocations, which makes the diffraction intensity of X-ray decreased and the diffraction spectrum broadens [28]. Result was that the amount of martensite in the first group was the lowest, and the result for the third group of martensite was the highest.

3.3. Residual Stress and Residual Austenite Analysis

As shown in Fig. 7, the varying degrees of residual compressive stress and RA were obtained in the cladding layer with three groups of different LTT alloy

Table 3. The wear weightlessness of change over time (g)

Time/min	S235	1#	2#	3#
15	0.162	0.005	0.003	0.005
30	0.285	0.008	0.005	0.009
60	0.513	0.013	0.009	0.015

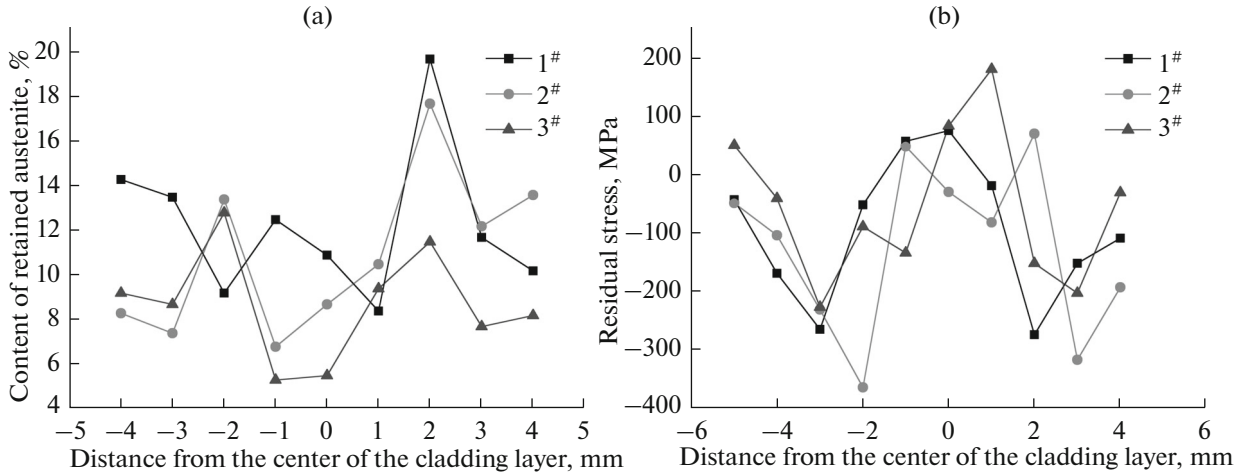

Fig. 7. Distribution curves of RS and RA in the cladding metal with three groups of different LTT alloy powder. (a) Retained austenite, (b)residual stress.

powder. From Fig. 7a, we can see that the amount of RA in the cladding layer of the 1# group is the maximum, about 12.17%. The transformation of austenite to martensite is the most adequate in the cladding layer of the 3# group, and only about 8.6% of RA is left in the cladding layer. The RA in the 2# group is about 10.85%. Figure 7b shows that the maximum compressive RS occurs in the region between the central and the side of the cladding metal. Because the undercooling of both sides is higher than that of the central region of the cladding metal during the solidification of molten metal, the central region is still in a state of melting or plastic during the solidification of the two sides. The solidification shrinkage of the two sides of the cladding metal is not restrained by the central region and does not form larger tensile stress. The solidification shrinkage of the central region is restrained and subjected to a large tensile stress by both sides of the metal that has been solidified, resulting small compressive RS and even tensile RS. Due to the high temperature of the arc, the elements diffusion phenomenon occurs in the vicinity of the fusion zone after the melting of the base material and the cladding layer during the deposition process. So the martensitic transformation temperature of the base metal near the fusion zone is reduced, resulting in the phase transformation expansion, and the compressive RS appears in a small range. The average compressive RS in the cladding layer of the 2# group of LTT powder is the largest, and the maximum can reach to −361 MPa. Because the metal element Cr, Ni can effectively increase the stability of the overcooling austenite and reduce the martensitic transformation temperature [29]. The Ms of the 1# group is the lowest and the 3# group is the highest. The austenite has more time to transform to martensite and the transition is more adequate with higher Ms of the cladding metal, resulting in the least amount of RA in the 3# groups, about 8.6%. The cladding metal is in a state of elastic plasticity with higher Ms and the volume expansion of the martensite transformation can be partially recovered. During the process of cooling to room temperature after the end of the martensitic transformation, the tensile stress generated by the thermal shrinkage of the cladding metal counteracts the compressive stress caused by the phase transformation expansion. So the average compressive RS is relatively smaller, about −229 MPa. The transformation of austenite to martensite is in a small temperature range with lower Ms of the cladding metal. There is not enough driving force for martensite transformation after cooling to room temperature in a relatively short time, resulting in more RA in the final cladding metal, about 12.17%. So the compressive stress generated by the phase transformation expansion is also relatively small. The maximum compressive RS of the cladding metal is about −267 MPa. Compared with the 1# and 3# groups, the larger compressive RS can be obtained by the expansion of the martensitic transformation in the 2# cladding metal. The maximum of the RS can reach −361 MPa.

3.4. Micro-Hardness Analysis of Cladding Layers

The Vickers hardness distribution curves of three groups with different LTT alloy powders from the argon arc cladding metal to the substrate is shown in Fig. 8. The hardness decreases with the increase of the distance from the surface of the cladding metal, and the fusion zone is the transition region. Compared with the matrix, the average hardness of the 1# group alloy powder increases by 2.1 times, the second group increases by 2.6 times, and the third group increases by 1.9 times. The hardness of the cladding metal is related to the number and morphology of martensite [30]. The finer and more the microstructure of martensite is, the higher the hardness of the cladding metal is.

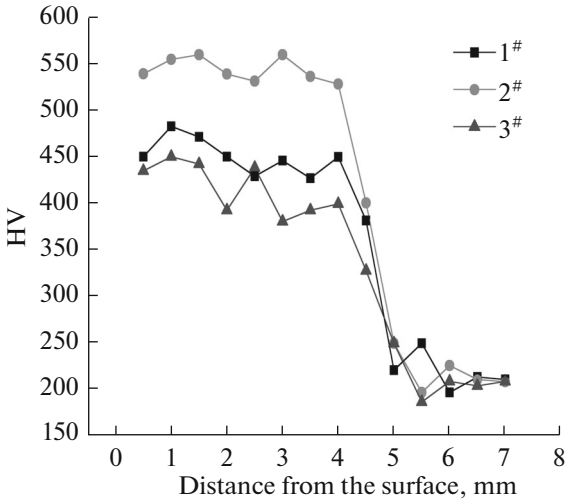

Fig. 8. Micro-hardness distribution of three groups of deposited layers.

The RS of cladding metal also has a great influence on the hardness [31]. When the pressure head of the micro hardness tester is pressed in, the cladding metal begins to enter the yield stage. When the RS in the deposited layer is tensile stress, the shear stress of the deposited layer is increased, leading to the increase of the plastic deformation and the decrease of the hardness. When the RS in the cladding metal is compressive stress, the shear stress can be reduced effectively, which will suppress the compression of the pressure head. Finally, the elastic plastic deformation of the cladding layer reduces, and the hardness increases. Although the martensite in the cladding metal of the 3# group is more than the 1# group and the cladding metal has many RA with lower hardness, deposited layer of compression RS is higher than that of the 3# group. Therefore, the hardness of the 1# group is higher than that of the 3# group. There are large quantities of relatively fine martensite grains in the cladding metal of the 2# group, which increases the grain boundary area and the ability to resist the dislocation. Therefore, the plastic deformation can be suppressed effectively. The compressive RS in the cladding metal is very large, which greatly reduces the shear stress when the pressure head is pressed into the cladding metal. So the elastic plastic deformation is very small and the overall hardness of the cladding metal is much higher than that of the other two groups. The hardness of recrystallization microstructure in the HAZ is significantly higher than that of the coarse grain in the overheated zone.

3.5. Wear Resistance Analysis

Table 3 shows the weight loss of the three groups of cladding metal and base metal with time. As shown in the table, the wear resistance of the cladding metal is

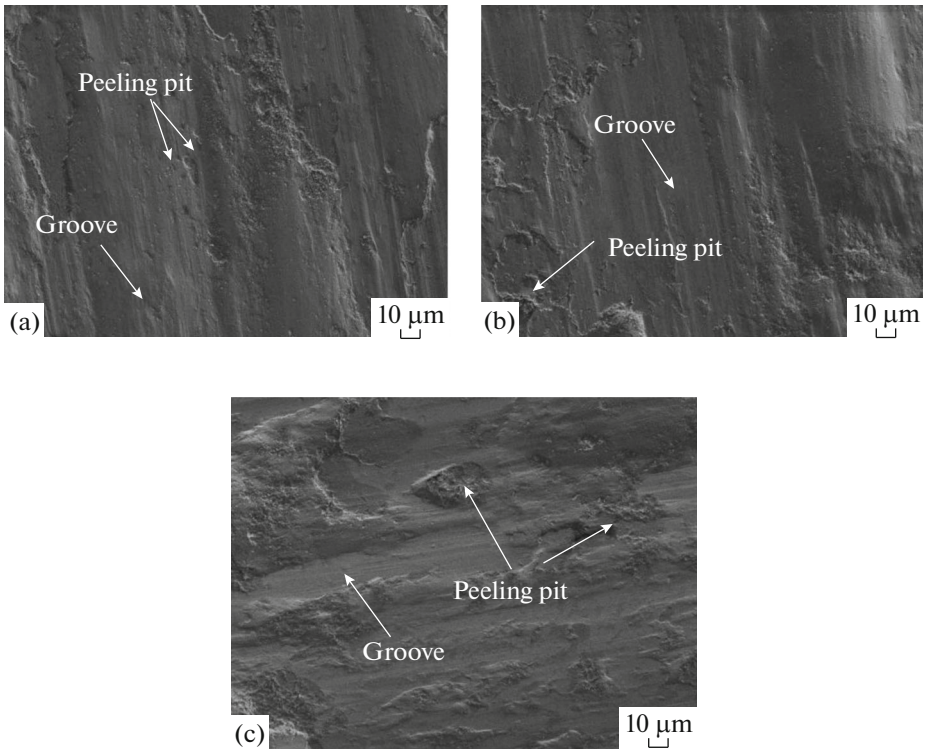

Fig. 9. SEM wear morphology of cladding metal. (a)12%Cr, 10%Ni, (b)10%Cr, 8%Ni, (c) 8%Cr, 6%Ni.

much higher than that of the base material S235. The wear weight loss grows greatly at the beginning, but decreases with the wear time. The friction pair is in contact with the surface of the cladding layer for just a very small part in the initial stage of wear, which resulted in a larger stress concentration, so the wear is larger. The contact area of the friction pair and the pattern surface is gradually increasing with the extension of wear time, leading to the decrease of the stress concentration. Plastic deformation occurred in the cladding metal due to the early friction, which resulted in the phenomenon of work hardening. The wear loss is lower than that of the initial wear stage. The microstructure of the cladding layers is mainly martensite and RA. On the one hand, martensite has high hardness and good wear resistance. A small amount of RA that distributed in the martensite has a very good toughness, which can effectively alleviate the stress caused by the friction pair and reduce the crack growth rate. Study shows that the presence of a proper amount of retained austenite can reduce the generation of welding crack [32]. On the other hand the compressive RS in the cladding metal can relax the stress concentration, reduce the shear stress on the surface of the cladding layer caused by the friction pair, and improve the wear resistance. So the wear resistance of the cladding metal is much higher than that of the base metal S235. Compared with the other two groups, the compressive RS of the cladding metal in group $2^{\#}$ was the maximum, which resulted in the best relaxation effect to the stress concentration. The $2^{\#}$ group has the best wear resistance.

SEM wear morphology of the deposited layer for the three groups is shown in Fig. 9. There are a lot of intermittent peeling pit with different sizes and grooves with different depth on the surface of the cladding metal in the three groups. Compared with the $2^{\#}$ group, the plow groove of the $1^{\#}$ group was deeper and the peeling pit of group $3^{\#}$ was the most serious. The contact area at the beginning between the friction pair and surface of the sample is very small. Under the action of normal load, the pressure of hard phase particles of the friction pair to contact position of the sample exceeds the yield strength and result in irreversible deformation, which leads to the form of strong adhesion between two friction surfaces. The adhesive part can be cut off under the action of shearing force as soon as the friction pair begins to move, thereby forming a sample of a concave surface. The cutting debris will become a new grinding grain together with the hard particles of friction pairs to plow the surface of the specimen, forming plough groove on the surface of the sample. The cladding layer of group $2^{\#}$ can be the best to suppress the pressure of the hard particles in the friction pairs and relax the shear stress on the surface of the sample caused by friction pairs due to the maximum residual compressive stress.

4. CONCLUSIONS

(1) The metallurgical bonding without defects between the base material and the low-temperature phase transformation coating prepared by the in-situ synthesis method of argon arc cladding has formed. The microstructure of the cladding layer is slab martensite and retained austenite distributed in the martensite.

(2) Three groups of low temperature transformation cladding layers have obtained varying degrees of residual compressive stress. The maximum compressive RS is −267 MPa($1^{\#}$), −361 MPa($2^{\#}$) and −229 MPa($3^{\#}$) respectively, which can effectively compensate the tensile stress caused by thermal shrinkage. The metal material is in the elastic-plastic state if the martensitic transformation temperature is relatively high, leading to partially restoration of the volume expansion after the end of the martensitic transformation and the tensile stress caused by the thermal shrinkage at the process of cooling to room temperature. Martensitic transformation is not sufficient if the martensitic transformation temperature is too low, resulting unable to obtain the maximum volume expansion. Therefore, the maximum compressive RS can be obtained with 10%Cr and 8%Ni.

(3) The compressive RS can reduce the shear stress and relax the stress concentration, which could improve the hardness and wear resistance of the cladding metal. Compared with the matrix materials, the hardness of the cladding metal of $1^{\#}$, $2^{\#}$ and $3^{\#}$ is increased by 2.1 times, 2.6 times and 1.9 times respectively. The wear resistance of the three groups are increased by 39 times, 57 times, and 34 times respectively.

ACKNOWLEDGMENTS

This work is sponsored by the National Natural Science Foundation of China under Grant no. 51575401, this work is partly sponsored by Zhejiang Provincial Natural Science Foundation (Grant no. LY16E050007), also is partly supported by State Key Lab of Advanced Welding and Joining, Harbin Institute of Technology (no. AWJ-16-M01). We appreciate Dr. Manda Yang from University of Pennsylvania help to polish the language which improved the paper quality.

REFERENCES

1. Y. Dong, Y. S. Zhang, and X. P. Lin, *Modern Surface Engineering Technology* (Mechanical Industry Press, Beijing, 2003) [in Chinese].
2. B. S. Xu, S. C. Liu, et al., *Plasma Spraying and Surfacing* (Chinese Railway Press, Beijing, 1986) [in Chinese].
3. D. Bartkowski and G. Kinal, Int. J. Refract. Met. Hard Mater. **58**, 157 (2016).
4. J. Yang, J. H. Huang, D. Y. Fan, and S. H. Chen, Mater. Des. **88**, 1031 (2015).

5. M. Sharifitabar, J. V. Khaki, and M. H. Sabzevar, Surf. Coat. Technol. **285**, 47 (2016).
6. D. Q. Chen, D. Liu, Y. F. Liu, H. M. Wang, and Z. Huang, Surf. Coat. Technol. **239** (239), 28 (2014).
7. F. X. Fu, Y. L. Zhang, G. R. Chang, and J. Dai, Optik (Munich, Ger.) **127** (1), 200 (2016).
8. D. Z. Wang, Q. W. Hu, and X. Y. Zeng, Surf. Coat. Technol. **274**, 51 (2015).
9. T. Shiozaki, Y. Tamai, and T. Urabe, Int. J. Fatigue **80**, 324 (2015).
10. A. A. Bhatti, Z. Barsoum, V. van der Mee, and A. Kromm, Procedia Eng. **66**, 192 (2013).
11. X. H. Zhao, D. P. Wang, and C. Y. Deng, Mater. Des. **53**, 490 (2014).
12. X. Z. Chen, J. J. Wang, Y. Y. Fang, M. Bruce, G. F. Xu, and J. Z. Zhou, Opt. Laser Technol. **57** (4), 159 (2014).
13. X. Z. Chen, Y. Y. Fang, S. Y. Zhang, J. F. Kelleher, and J. Z. Zhou, Fusion Eng. Des. **27** (1), 54 (2015).
14. X. Z. Chen, S. Y. Zhang, J. J. Wang, and J. F. Kelleher, Mater. Des. **76**, 26 (2015).
15. T. Shi, X. C. Li, and Z. T. Liu, *The Physical Properties of Metal* (Aviation Industry Press, Beijing, 1994) [in Chinese].
16. S. W. Ooi, J. E. Garnham, and T. I. Ramjaun, Mater. Des. **56** (4), 773 (2014).
17. Z. Barsoum and M. Gustafsson, Eng. Failure Anal. **16** (7), 2186 (2009).
18. X. Z. Chen, Y. Y. Fang, P. Li, Z. Z. Yu, X. D. Wu, and D. S. Li, Mater. Des. **65**, 1214 (2015).
19. A. S. N. Ohta, Y. Maeda, K. Hiraoka, and T. Nakamura, Int. J. Fatigue **21** (99), 113 (1999).
20. A. W. O. Ohta, K. Matsuoka, C Shiga, S. Nishijima, Y. Maeda, N. Suzuki, and T. Kubo, Weld. World **43**, 38 (1999).
21. F. MD, Weld. World **43**, 63 (2008).
22. D. Camilleri and N. McPherson, Sci. Technol. Weld. Joining **110** (10), 2 (2013).
23. Y. Mikami, Y. Morikage, M. Mochizuki, and M. Toyoda, Sci. Technol. Weld. Joining **14** (2), 97 (2009).
24. T. Angel, J. Iron Steel Inst., London **177**, 165 (1954).
25. J. Janssen, M. Follon, and L. Delaey, *Strength of Metals and Alloys,* Ed. by P. Haasen (Pergamon Press, London, 1979).
26. W. Steven and A. G. Haynes, J. Iron Steel Inst. **20**, 349 (1956).
27. Q. P. Wang, W. S. Li, Welding **11**, 8 (2004).
28. Y. G. Min, J. F. Zhao, J. P. Lin, and J. Y. Min, J. Tongji Univ., Nat. Sci. **01**, 113 (2016).
29. M. A. Kromm and T. Kannengiesser, Weld. World **55** (3–4), 48 (2011).
30. S. V. Konovalov, V. E. Kormyshev, V. E. Gromov, et al., J. Surf. Invest.: X-ray, Synchrotron Neutron Tech. **10** (5), 1119 (2016).
31. L. Zhang, J. Z. Lu, K. Y. Luo, A. X. Feng, F. Z. Dai, J. S. Zhong, M. Luo, and Y. K. Zhang, Mater. Sci. Eng., A **561** (3), 136 (2013).
32. H. Sakamoto, Y. Kijima, and K. Shimizu, Trans. Jpn. Inst. Met. **23** (10), 585 (1982).